Kinetics and Mechanism of the Acetylperoxy + HO_2 Reaction

Mary A. Crawford,† Timothy J. Wallington, Joseph J. Szente, and M. Matti Maricq*

Research Laboratory, Ford Motor Company, P.O. Box 2053, Drop 3083, Dearborn, Michigan 48121

Joseph S. Francisco

Department of Chemistry, Purdue University, West Lafayette, Indiana 47907-1397

Received: July 23, 1998; In Final Form: November 5, 1998

The reaction of HO_2 with $CH_3C(O)O_2$ is examined using flash photolysis and FTIR smog chamber techniques. Time-resolved UV spectroscopy is used to follow the transient peroxy species. It yields reasonable concentration versus time profiles for $CH_3C(O)O_2$ and HO_2, but indicates anomalously high levels of secondary CH_3O_2 radicals. Transient IR diode laser absorption confirms the HO_2 decay rates; however, the anticipated reaction model substantially underestimates the observed decay. The model is augmented by assuming that, in analogy with formaldehyde, there exists a reaction between HO_2 and acetaldehyde (the precursor for $CH_3C(O)O_2$). Consistent with this, the fitted rate for the hypothesized reaction increases with increasing initial acetaldehyde level. Relative rate measurements reveal that chlorine atoms remove more CH_3CHO relative to CH_3OH in air as compared to nitrogen diluent. This supports the hypothesis since, in the presence of oxygen, HO_2 is formed and presents an additional acetaldehyde removal pathway. Employing the augmented model, analyses of HO_2 decay traces yield a $CH_3C(O)O_2 + HO_2$ rate constant of $k_1 = (3.9^{+5.0}_{-2.3}) \times 10^{-13} e^{(1350\pm250)/T}$ cm^3 s^{-1}. Reasons are discussed for why the present rate constants are 2−3 times larger than previously reported. FTIR−smog chamber studies reveal the reaction to proceed via two channels to (a) peracetic acid and O_2 and to (b) acetic acid and O_3 , with a branching fraction at 295 K that is less than half of the literature value. Time-resolved UV absorption measurements support this smaller fraction; averaged together the two methods give $k_{1b}/k_1 = 0.12 \pm 0.04$. As part of this work, relative rate techniques are used to measure $k(Cl+CH_3C(O)OH) = (2.5 \pm 0.3) \times 10^{-14}$ cm^3 s^{-1} and $k(Cl+CH_3C(O)OOH) = (4.5 \pm 1.0) \times 10^{-15}$ cm^3 s^{-1} at 295 K.

I. Introduction

Acetylperoxy radicals appear in the atmosphere as intermediates in the photooxidation of a variety of anthropogenic and biogenic compounds. It has been well established that this radical plays an important role in determining ambient peroxyacetylnitrate (PAN) concentrations.[1−3] PAN, a ubiquitous compound found in photochemical smog, is formed by the reaction of $CH_3C(O)O_2$ with NO_2 . The stability of this adduct against thermal decomposition exhibits a strong temperature dependence. At low temperatures, PAN effectively sequesters both NO_2 and a peroxy radical and, thereby, manifests a significant influence on ozone formation. Furthermore, owing to its relative stability, PAN provides a vehicle for long-range transport of reactive nitrogen from urban areas where NO_x concentrations tend to be high to rural areas having relatively low NO_x levels.

As a result of its importance as a member of the odd nitrogen group, there have been a number of measurements of urban and rural PAN concentrations. Recently, Shepson et al.[4] and Hartsell et al.[5] have explored the relationships between PAN, ozone, and NO_y in sites in Ontario, Canada and as part of the Southern Oxidants Study in the Southeast United States, respectively. Both studies observe diurnal variations in the $[O_3]$/[PAN] ratio that indicate nighttime PAN concentrations to decrease faster than those of ozone. They find this somewhat surprising since at night $[NO_2]$/[NO] is generally high and [NO] is relatively low; thus, one would surmise that both the net loss of PAN via thermal decomposition and the loss of ozone via titration with NO would be slow. Both groups suggest that the nighttime increase in the $[O_3]$/[PAN] ratio arises from a higher deposition velocity for PAN as compared to ozone.

Atmospheric simulations by Stockwell et al.[6] suggest a different explanation. Using a box model, they found that PAN concentrations are sensitive to a number of peroxy radical reactions, notably the acetylperoxy radical/HO_2 reaction, along with the $CH_3C(O)O_2$ reactions with itself, NO, and CH_3O_2 . Stockwell et al.[6] further indicate that PAN decomposition through the $CH_3C(O)O_2$ intermediate can be important even if the $[NO_2]$ to [NO] ratio is high and conclude that this is a viable alternative to deposition for explaining the observed diurnal variation in the $[O_3]$/[PAN] ratio. However, despite their potential significance for understanding tropospheric PAN chemistry, the reactions of the acetylperoxy radical have received relatively little attention, particularly those reactions with other peroxy radicals.

Recent measurements of PAN and NO_2 over the southern United States suggest that the concentration of $CH_3C(O)O_2$ radicals in the free troposphere is typically $(1-10) \times 10^4$ cm^{-3}.[7] The most important of the atmospheric peroxy radical/peroxy radical reactions of $CH_3C(O)O_2$ is its reaction with HO_2 .[6] Niki et al.[8] were the first to examine this reaction and their product study showed it to proceed via two channels:

* Author for correspondence.
† On leave from Department of Chemistry, Purdue University. Present address: Knox College, Galesburg, IL 61401.

10.1021/jp983150t CCC: $18.00
Published on Web 01/05/1999

$$CH_3C(O)O_2 + HO_2 \rightarrow CH_3COO_2H + O_2 \quad (1a)$$

$$CH_3C(O)O_2 + HO_2 \rightarrow CH_3COOH + O_3 \quad (1b)$$

with branching fractions of 0.75 and 0.25 for channels 1a and 1b, respectively. In a subsequent kinetic study, Moortgat et al.[9] reported the somewhat higher yield of 0.33 for channel 1b. Horie et al.[10] also investigated the $CH_3C(O)O_2 + HO_2$ reaction by photolyzing biacetyl in the presence of O_2 and analyzing the reaction products utilizing matrix-isolation FTIR spectroscopy. They confirmed the production of ozone and determined the temperature dependence of the branching ratio over the 263−333 K range. The only direct kinetic investigation of the $CH_3C(O)O_2 + HO_2$ reaction is that of Moortgat et al.[9] Although based on limited data, the results suggest that the reaction is fast and has a steep negative temperature dependence with $E_a \cong 1040$ K^{-1}.

The rate constants and branching ratios measured in the present work differ significantly from those reported previously. Our time-resolved UV spectra could not be deconvoluted to yield sensible levels of the secondary methylperoxy radical. Possibly, this was due the difficulty in separating the contributions of three peroxy radicals, HO_2, $CH_3C(O)O_2$, and CH_3O_2, ozone, and long-lived reaction products to the UV spectra of the reaction mixture. Therefore, independent measurements of the $[HO_2]$ decay were undertaken using transient IR absorption. The IR data confirmed the UV determinations of the HO_2 concentrations, but the resultant $[HO_2]$ decay was as much as 7 times faster than anticipated and could only be fit upon augmenting the standard kinetic model with a reaction between HO_2 and acetaldehyde. Data from the smog chamber experiments also suggest that such a reaction takes place. The present experiments, techniques, and analysis, are discussed in detail in the following two sections. A comparison of our results to those of Moortgat et al.[9] is given in Section IV.

II. Experimental Section

A. Kinetic Measurements. The kinetics of the $CH_3C(O)O_2 + HO_2$ reaction is investigated over the 270−360 K temperature range. The peroxy radical reactants are generated by the photolysis of molecular chlorine in $Cl_2/CH_3OH/CH_3CHO/O_2/N_2$ gas mixtures using 10 ns, 300−600 mJ, 351 nm light pulses from an excimer laser. The gas mixture flows through a temperature-controlled cylindrical cell having a diameter of 3.2 cm and a path length of 51 cm. Gas flow rates are controlled using Tylan flow controllers with the exception of Cl_2 whose flow rate is regulated through a needle valve. Nitrogen is added to achieve the desired total pressure.

The reactant acetylperoxy and hydroperoxy radicals are formed after chlorine atoms released by photolysis abstract hydrogen atoms from the acetaldehyde and methanol precursors; thus,

$$Cl + CH_3CHO \rightarrow CH_3CO + HCl \quad (2)$$

$$CH_3CO + O_2 + M \rightarrow CH_3C(O)O_2 + M \quad (3)$$

$$Cl + CH_3OH \rightarrow CH_2OH + HCl \quad (4)$$

$$CH_2OH + O_2 \rightarrow CH_2O + HO_2 \quad (5)$$

The precursor and oxygen levels are made sufficiently high to ensure that these reactions are complete on a microsecond time scale, fast compared to the ensuing peroxy radical reactions.

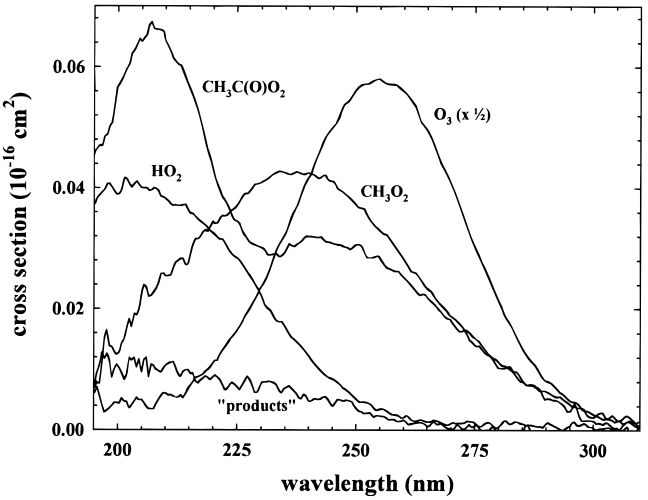

Figure 1. UV reference spectra of the principal species contributing to the absorbance spectra of the $CH_3C(O)O_2 + HO_2$ reaction mixture. Reference spectra are obtained as follows: $CH_3C(O)O_2$, ref 23; HO_2, ref 16; CH_3O_2, ref 11; O_3, unpublished; "products", present work.

Two methods are employed to follow the reaction, time-resolved UV spectroscopy and transient IR absorption. Both have been described previously.[11−13] In the former technique, broadband UV light from a D_2 lamp counterpropagates though the reaction cell and is dispersed by a 0.32 m monochromator with a 147 groove/mm grating onto a gated diode array detector. This configuration allows the UV absorption of the peroxy radicals to be monitored over the 200−300 nm wavelength range. Transient spectra are recorded by gating the detector at various times in the 0−1 ms range following the photolysis pulse. A time resolution of 10 μs is typical.

Time-dependent peroxy radical concentrations are determined by deconvolution of the absorbance versus wavelength traces according to

$$\text{abs}(t) = \sum [x_i]_t \sigma(x_i) l \quad (I)$$

where l represents the path length and the index $i = 1-5$ accounts for the hydroperoxy, acetylperoxy, methylperoxy, ozone, and "products" contributions to the overall absorbance. The relevant reference spectra are illustrated in Figure 1. While recommended cross sections for HO_2, O_3, and CH_3O_2 are available from literature reviews,[14] the recommended $CH_3C(O)O_3$ spectrum is not up to date, and that for "products" is unavailable. Thus, for consistency, all the reference spectra are collected with the same spectrometer as used for the kinetic measurements. A contribution to the absorbance from methylperoxy is included, since these radicals are secondary products of the acetylperoxy self-reaction. Ozone is included because it is formed by reaction 1b and absorbs strongly at 254 nm. "Products" accounts for UV absorption by reaction products such as H_2O_2 , CH_3OOH, and $CH_3C(O)OOH$, the first two of which begin to absorb weakly below about 230 nm[15] and the last of which is assumed to absorb in the same region by analogy. It is important to include the "products" term in eq I to distinguish its contribution to the absorbance from that of HO_2, which, having a peak cross section at 203 nm, also contributes in this spectral region;[16] thus, omission of the "products" term invariably leads to apparent HO_2 concentrations that decay to a nonzero level. The "products" reference spectrum is obtained by subtracting the ozone contribution from the absorbance of the reaction mixture at 20 ms, by which time the radical concentrations have decayed to 0.

Because of potential difficulties in deriving reliable concentrations by deconvoluting the rather complex UV absorbance spectra obtained for the reaction mixture (compare Figure 1 and Figure 3 below), the second method of transient IR absorption was used for independent measurement of the HO_2 concentration following its generation by flash photolysis. These experiments were, in a number of cases, run back-to-back under the same conditions as a corresponding UV measurement. With this technique, narrow band IR radiation from a Pb salt diode laser replaces the UV light provided by the D_2 lamp and is directed onto a HgCdTe detector with a 0.3 μs response time. A vibration-rotation line in the ν_3 O−O stretching band that conveniently falls between a pair of ammonia lines at 1117.45 and 1117.64 cm^{-1} is used to monitor the HO_2 concentration. The cross section of the HO_2 probe line is measured in a companion experiment in which the acetaldehyde is omitted from the reaction mixture; thus, all of the radicals are converted into HO_2 . Because the experiments are carried out in the pressure-broadening regime, the cross section varies with temperature, pressure, and the nature of the diluent gas. As a point of reference, it is 1.0×10^{-18} cm^2 at 295 K and 52 Torr of N_2 . Although the measurement precision is about 5%, the cross sections are calibrated against the concentration of ethylperoxy radicals; thus, the overall accuracy is about 10%.

Concentration versus time data are extracted from the transient absorption measurements via

$$\frac{dV(t)}{dt} = V_0 \frac{d}{dt} e^{-[HO_2]_t \sigma_{HO_2} l} - k_{det} V(t) \qquad \text{(II)}$$

a modified version of Beers Law that accounts for the ac coupling of the detector. Here, $V(t)$ represents the detector signal, l is the path length, and σ_{HO_2} is the IR cross section of the HO_2 vibration−rotation line. Because the detector is an AC-coupled device, there is a decay constant of $k_{det} = 300$ s^{-1} for the detector output to return to zero after its initial response to a step function change in light intensity. This term makes a small but noticeable contribution to the HO_2 decay over the 1 ms time scale of the present experiments, which primarily affects the determination of the HO_2 + CH_3CHO reaction rate.

As has been done previously,[11−13] the concentration of chlorine atoms generated by the photolysis pulse is calibrated by substitution of ethane for the acetaldehyde and methanol precursors under otherwise identical experimental conditions and recording the number of ethylperoxy radicals that are generated. The same procedure is used for measuring the total initial radical concentration in the $CH_3C(O)O_2$ + HO_2 kinetics experiments and for determining the HO_2 IR cross section. In this study, the total radical concentration varies from 5×10^{14} to 11×10^{14} cm^{-3} and the $[HO_2]_0/[CH_3C(O)O_2]_0$ ratio ranges from 0.7 to 3.

The temperature of the cell and reaction mixture is controlled by a Neslab ULT-80dd recirculating chiller that precools/preheats the gases, with the exception of acetaldehyde, before their entrance into the reaction vessel. Acetaldehyde is introduced just prior to the cell entrance to prevent its condensation on the walls of the gas manifold at the lowest temperatures employed. Acetaldehyde (99%) and methanol (99.9%) are acquired from Fisher. Nitrogen (99.999%), oxygen (ultrazero grade, THC < 0.5 ppm), and ethane (99.5%) are purchased from Michigan Airgas. Chlorine (4.8% in nitrogen) is obtained from Matheson. All the reagents are used without further purification.

B. FTIR−Smog Chamber System. Three sets of experiments using the FTIR system are reported. First, the kinetics of the reaction of Cl atoms with $CH_3C(O)OH$ and $CH_3C(O)OOH$ are studied using a relative rate method. Second, the reaction between HO_2 radicals and CH_3CHO is investigated using the irradiation of $CH_3CHO/^{13}CH_3OH/Cl_2$ mixtures in 700 Torr of either O_2 or N_2 diluent. Finally, the yields of $CH_3C(O)OH$ and $CH_3C(O)OOH$ are quantified following the irradiation of $CH_3CHO/CH_3OH/Cl_2$/air mixtures to determine the branching ratio for reaction 1.

The apparatus for these experiments consists of an FTIR spectrometer interfaced to a 140-L Pyrex reactor.[17] As with the kinetics experiments, radicals are generated by the UV irradiation ($\lambda > 300$ nm) of molecular chlorine in the presence of CH_3CHO and CH_3OH, in this case using 22 fluorescent blacklamps (GTE F40BLB). The experiments are performed at 295 K in the presence of 700 Torr of ultrahigh purity air or N_2 diluent. With only nitrogen present, hydrogen abstraction by the chlorine atoms produces CH_3CO and CH_2OH radicals. When O_2 is also present, these are rapidly converted to $CH_3C(O)O_2$ and HO_2 radicals. Initial concentrations of the gas mixtures used in this study were 30−230 mTorr of CH_3CHO, 200−300 mTorr of Cl_2, and 0−140 mTorr of CH_3OH in 700 Torr of air diluent (ultrahigh purity). The $[CH_3OH]/[CH_3CHO]$ concentration ratio was varied over the range 0−6.7. The rate constant ratio $k_2/k_4 = 1.5$; thus, the initial rate of HO_2 radical production is 0−4.5 times that of $CH_3C(O)O_2$ radicals.[18]

The loss of CH_3CHO and the formation of products are monitored using FTIR spectroscopy. Products are quantified by fitting reference spectra of the pure compounds to the observed product spectra using integrated absorption features over the 800−2000 cm^{-1} range. The IR path length is 28 m, the spectral resolution is 0.25 cm^{-1}, and spectra are derived from 32 coadded interferograms. Reference spectra are acquired by expanding known volumes of the reference compounds into the chamber.

The acquisition of reference spectra for $CH_3C(O)OH$ and $CH_3C(O)OOH$ is complicated by dimerization of acetic acid and the fact that the peracetic acid is supplied as a 32 wt % solution in acetic acid. The vapor above the liquid peracetic acid sample is ≅70% peracetic acid and ≅30% acetic acid dimer and monomer. There is no evidence for dimerization of the peracetic acid. The vapor above liquid acetic acid contains both monomer and dimer. The monomer exhibits IR absorptions centered at 991, 1184, 1275, 1385, and 1790 cm^{-1}, while the dimer has features at 944, 1294, 1426, 1731 cm^{-1}. Experiments were performed to study the equilibrium between monomer and dimer using a small (300 cm^3) Pyrex reaction cell filled with 0.27−3.95 Torr of $CH_3C(O)OH$ vapor (both monomer and dimer). As expected, the concentration of dimer varies in proportion to the square of the monomer concentration. A value of $K_{eq} = [\text{dimer}]/[\text{monomer}]^2 = 2.5 \pm 0.3$ $Torr^{-1}$ is derived at 295 K and 700 Torr of N_2 diluent. This result is consistent with the available literature data.[19] Quantification of the $CH_3C(O)OH$ and $CH_3C(O)OOH$ absorption intensities is achieved using $\sigma(CH_3C(O)OH \text{ monomer}) = 5.9 \times 10^{-19}$ cm^2 at 1177 cm^{-1}, $\sigma(CH_3C(O)OH \text{ dimer}) = 1.80 \times 10^{-18}$ cm^2 at 1295 cm^{-1}, and $\sigma(CH_3C(O)OOH) = 1.81 \times 10^{-19}$ cm^2 at 1251.5 cm^{-1}. Systematic uncertainties associated with these calibrations are estimated to be <10% for $CH_3C(O)OH$ and <15% for $CH_3C(O)OOH$. The reference spectra used in this work are given in Figure 2.

III. Results

A. Kinetic Measurements of k_1. This section describes the real-time kinetics measurements of the HO_2 + $CH_3C(O)O_2$ reaction rate constant. The results of the product study are presented in Section III.B. Figure 3 shows a typical UV

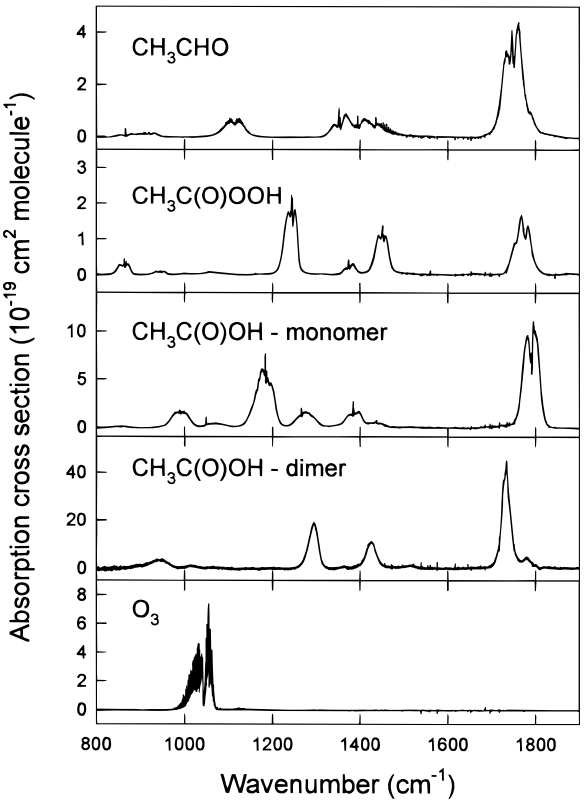

Figure 2. IR reference spectra used for the FTIR product study.

absorbance−wavelength−time surface obtained following photolysis of a $CH_3CHO/CH_3OH/Cl_2/O_2/N_2$ gas mixture. Qualitatively, the spectrum undergoes the expected changes in time. Initially, it exhibits a dominant peak at about 210 nm with a shoulder at 250 nm, which, according to the reference spectra in Figure 1, is consistent with a mixture of $CH_3C(O)O_2$ and HO_2 radicals (essentially formed instantaneously by the photolyzed Cl atoms). As time progresses, the 210 nm peak intensity decreases rapidly, since both the acetylperoxy and hydroperoxy radicals exhibit strong absorption features in this wavelength region and both are lost due to radical/radical reactions. The principal loss pathways include the $CH_3C(O)O_2 + HO_2$ reaction under investigation, as well as the self-reactions

$$HO_2 + HO_2 \rightarrow H_2O_2 + O_2 \quad (6)$$

$$CH_3C(O)O_2 + CH_3C(O)O_2 \rightarrow 2\,CH_3C(O)O + O_2 \quad (7)$$

In contrast, the absorbance at 250 nm decreases more slowly, giving the spectrum a flatter appearance at longer times. Unlike at 210 nm, the loss of intensity in this spectral region does not depend on the HO_2 concentration. Intensity lost due to a decrease in $CH_3C(O)O_2$ concentration is partly compensated by absorption due to CH_3O_2 radicals formed from the products of reaction 7 via

$$CH_3C(O)O \rightarrow CH_3 + CO_2 \quad (8)$$

$$CH_3 + O_2 + M \rightarrow CH_3O_2 + M \quad (9)$$

and from the ozone produced by reaction 1b. Ozone and the secondary methylperoxy radicals complicate analysis of the UV absorption data. A generic "products" category is added to account for the peroxide products of reactions 1a and 6 and from secondary reactions described in Table 1,[20] bringing to five the number of species contributing to the overall UV absorbance. By 500 μs, the acetylperoxy and hydroperoxy radicals have largely disappeared and the spectrum is dominated by methylperoxy, ozone, and "product" absorptions. As explained in Section II, omitting the "products" contribution to the absorbance leads incorrectly to apparent nonnegligible concentrations of HO_2 at long times.

Although Figure 1 shows that the spectra of the five contributing species overlap considerably, recording the complete wavelength dependence of the absorbing reaction mixture affords a reasonable prospect of extracting concentration versus time profiles for the individual constituents. Deconvolution of the spectral surface in Figure 3 according to eq I yields the concentration traces illustrated in Figure 4. Predictions from the model of Table 1 and based on the rate constants described below are in good agreement with the rapid decay observed in $CH_3C(O)O_2$ and HO_2 levels and with the production of O_3; however, they underestimate by about a factor of 2 the extent of CH_3O_2 formation. It is possible that this problem originates from difficulties in separating the contributions of the five constituents to the overall absorbance. However, the fact that a large discrepancy appears for the methylperoxy concentration, whereas the others are correctly predicted, suggests that something may be missing from the postulated reaction mechanism.

The IR diode laser probe provides an independent assessment of the amount of HO_2 in the reaction mixture and permits us to ascertain the accuracy of concentrations extracted from the time-resolved UV absorbances. Consistency between the IR and UV determinations of HO_2 has been demonstrated by our previous study of the HO_2 + c-$C_5H_9O_2$ reaction.[21] Figure 5 illustrates the results for the present reaction with $CH_3C(O)O_2$. The inset reveals good agreement between the UV (symbols) and IR (line) derived HO_2 levels. Although the acetylperoxy radical is not independently probed in the IR, the predictions based on the value of k_1 found from fitting the HO_2 IR data are in good agreement with the UV-based $CH_3C(O)O_2$ measurements and indirectly corroborate the UV data.

The main part of Figure 5 compares two model predictions to the IR-derived HO_2 concentrations. The dashed line represents the best fit using a model consisting of reactions 1 and 6−9 and the secondary reactions of the methylperoxy radical with HO_2 , $CH_3C(O)O_2$, and itself. This model cannot account for the shape of the hydroperoxy radical decay for any of the experiments in this study. If, as shown in the figure, the initial decay rate is in reasonable agreement with the data, then the overall loss is underestimated. Alternatively, the overall loss of HO_2 could be brought into agreement by raising k_1 , but then the model would considerably overestimate the initial decay rate.

One feasible explanation for this behavior is that an unanticipated secondary species reacts with HO_2 causing larger removal at longer times than predicted by the model. This explanation, however, falls short in two respects. First, at the 10^{14} cm^{-3} radical concentrations of these experiments, sufficient HO_2 removal by a secondary species would require an unrealistically large rate constant. Second, this hypothesis fails to account for the anomalously high methylperoxy levels observed from the UV absorbance measurements.

Potentially, another explanation for the higher than expected CH_3O_2 levels involves the possible recycling of $CH_3C(O)O_2$ radicals by the reaction of secondary methoxy radicals with acetaldehyde ($k = 7.4 \times 10^{-14}$ cm^3 s^{-1}),[22]

$$CH_3O + CH_3CHO \rightarrow CH_3CO + CH_3OH \quad (10)$$

In the present mechanism (Table 1), methoxy radicals arise from the cross reaction of acetylperoxy radicals with CH_3O_2 and from

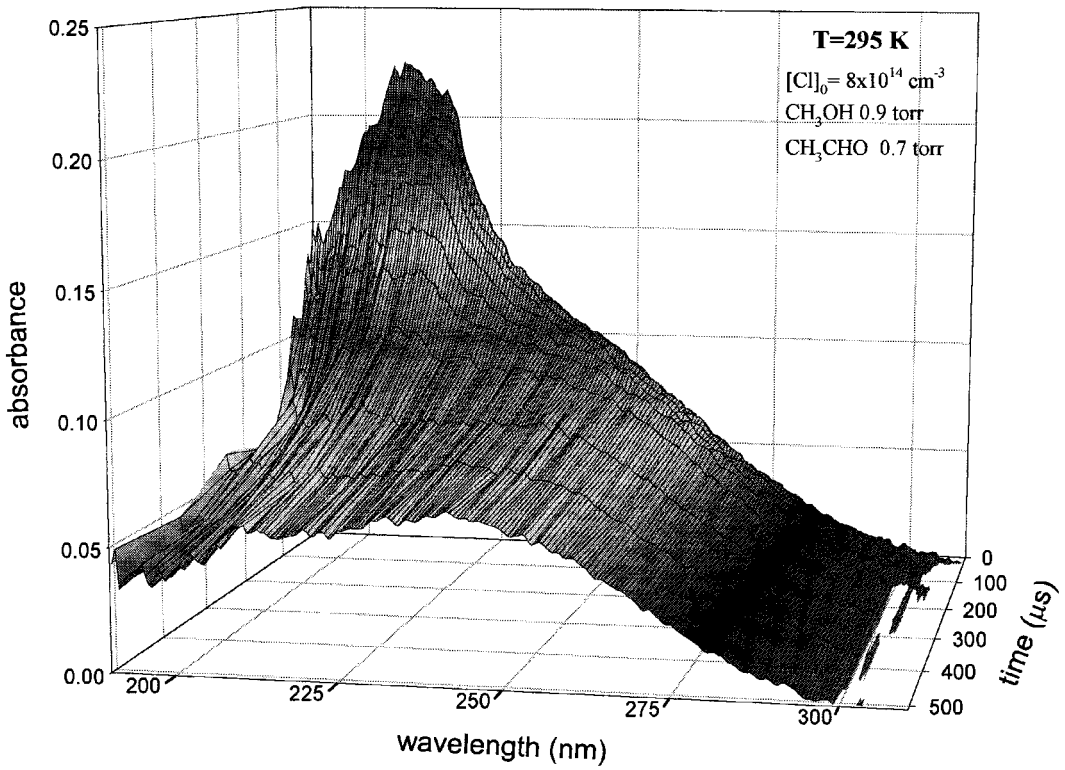

Figure 3. Time-resolved UV absorbance of a $CH_3CHO/CH_3OH/Cl_2/O_2/N_2$ reaction mixture following 351 nm photolysis.

TABLE 1: $CH_3C(O)O_2$ + HO_2 Reaction Mechanism

reaction	rate constant[a]
Principal	
(1a) $CH_3C(O)O_2 + HO_2 \rightarrow CH_3C(O)OOH + O_2$	$k_1 = 3.9 \times 10^{-13}e^{1350/T}$ cm^3 s^{-1} [b]
(1b) $CH_3C(O)O_2 + HO_2 \rightarrow CH_3COOH + O_3$	$k_{1b}/k_1 = 0.12$[b]
(6) $HO_2 + HO_2 \rightarrow H_2O_2 + O_2$	$k_6 = 2.8 \times 10^{-13}e^{(594/T)}$ cm^3 s^{-1} 16
(7) $CH_3C(O)O_2 + CH_3C(O)O_2 \rightarrow 2\ CH_3C(O)O + O_2$	$k_7 = 3.0 \times 10^{-12}e^{504/T}$ cm^3 s^{-1} 13
(13) $HO_2 + CH_3CHO \rightarrow CH_3C(OH)HO_2$	$k_{13} \cong 5 \times 10^{-14}$ cm^3 s^{-1} [b]
Secondary	
(8) $CH_3C(O)O \rightarrow CH_3 + CO_2$	$k_8 > 1 \times 10^6$ s^{-1}
(9) $CH_3 + O_2 + M \rightarrow CH_3O_2 + M$	$k_9 = 4.5 \times 10^{-31}(T/300)^{-3}$ cm^6 s^{-1} 15
(11a) $CH_3C(O)O_2 + CH_3O_2 \rightarrow CH_3C(O)O + CH_3O + O_2$	$k_{11a} = 0$ cm^3 s^{-1} 23,[c]
(11b) $CH_3C(O)O_2 + CH_3O_2 \rightarrow CH_3COOH + CH_2O + O_2$	$k_{11b} = 8.5 \times 10^{-13}e^{726/T}$ cm^3 s^{-1} 23
$HO_2 + CH_3O_2 \rightarrow CH_3OOH + O_2$	$k = 4.1 \times 10^{-13}e^{(790/T)}$ cm^3 s^{-1}
$HO_2 + CH_3C(OH)HO_2 \rightarrow$ products	assumed = $k_{CH_3O_2+HO_2}$
$CH_3C(O)O_2 + CH_3C(OH)HO_2 \rightarrow$ products	assumed = $k_{CH_3C(O)O_2+CH_3O_2}$
Tertiary	
$HO_2 + CH_2O \rightarrow CH_2(OH)O_2$	$k = 9.71 \times 10^{-15}e^{(625/T)}$ cm^3 s^{-1}
(12a) $CH_3O_2 + CH_3O_2 \rightarrow 2\ CH_3O + O_2$	$k_{12a} = (1 - b) \times 9.1 \times 10^{-14}e^{416/T}$ cm^3 s^{-1}
(12b) $CH_3O_2 + CH_3O_2 \rightarrow CH_3OH + CH_2O + O_2$	$k_{12b} = b \times 9.1 \times 10^{-14}e^{416/T}$ cm^3 s^{-1}
	$b = (1 + 25 \times e^{-1165/T})^{-1}$
$CH_3O_2 + CH_3O \rightarrow CH_2O + CH_3OOH$	$k = 1.5 \times 10^{-12}$ cm^3 s^{-1}
$CH_3O + CH_3O \rightarrow CH_2O + CH_3OH$	$k = 3 \times 10^{-11}$ cm^3 s^{-1}
$CH_3O + O_2 \rightarrow CH_2O + HO_2$	$k = 3.9 \times 10^{-14}e^{-900/T}$ cm^3 s^{-1}

[a] Rate constants taken from ref 15 unless otherwise noted. [b] Measured in the present study. [c] Branching fraction varied from 0 to 1 to establish sensitivity on k_1 determination.

the self-reaction of the latter species,

$$CH_3C(O)O_2 + CH_3O_2 \rightarrow CH_3C(O)O + CH_3O + O_2 \quad (11a)$$

$$\rightarrow CH_3COOH + CH_2O + O_2 \quad (11b)$$

$$CH_3O_2 + CH_3O_2 \rightarrow 2CH_3O + O_2 \quad (12a)$$

$$\rightarrow CH_3OH + CH_2 + O_2 \quad (12b)$$

Because it is slow and involves two secondary species, the methylperoxy self-reaction produces only a negligible quantity of methoxy radicals over the 1000 μs time scale of the present experiments. There is currently disagreement in the literature over the branching of reaction 11.[10,23,24] However, model simulations show that the maximum recycling is less than about 5% of the initial $CH_3C(O)O_2$ concentration, even if reaction 11 proceeds entirely via channel 11a; thus, the recycling mechanism cannot explain the difficulty in fitting the HO_2 decay in Figure 5.

Another possibility is that HO_2 reacts with acetaldehyde. This reaction was postulated by Moortgat et al.[25] in analogy with the known reaction between HO_2 and formaldehyde.[26] It would form an adduct that rearranges to the 1-hydroxy ethylperoxy radical; thus,

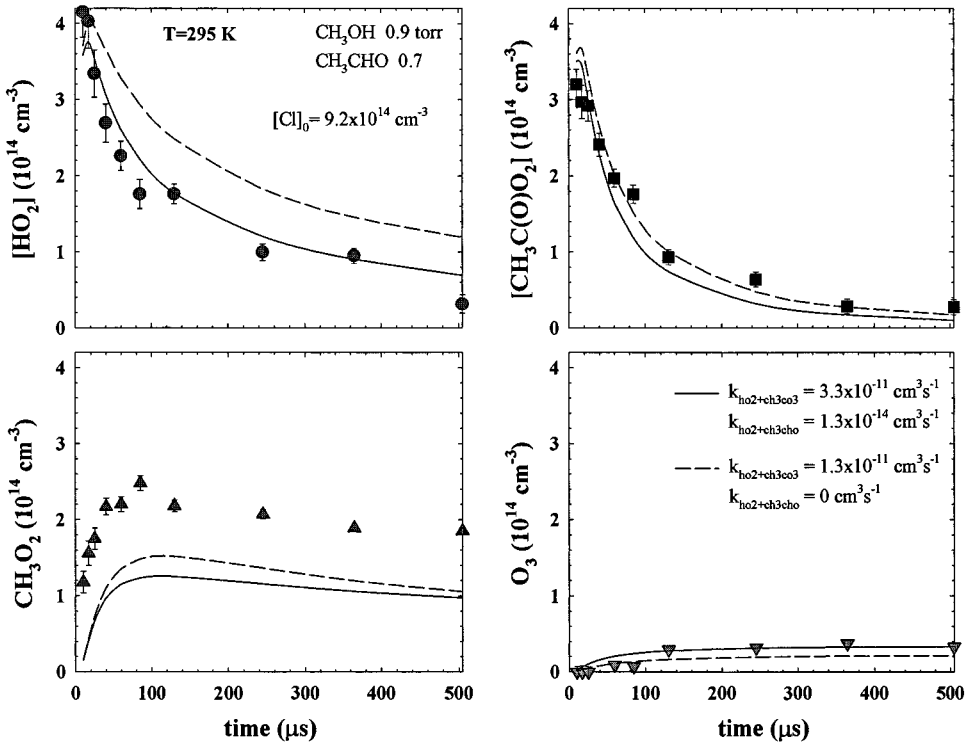

Figure 4. Concentration versus time profiles for HO_2 , $CH_3C(O)O_2$, CH_3O_2 , and O_3 as obtained from deconvolution of the spectral surface illustrated in Figure 3. The solid lines represent predictions from the reaction model of Table 1. The dashed lines are obtained assuming the value for k_1 reported by Moortgat et al.[9] The error bars are 95% confidence limits for the deconvolution. The actual errors are somewhat larger, ~10%, owing to the systematic uncertainty in the reference cross sections.

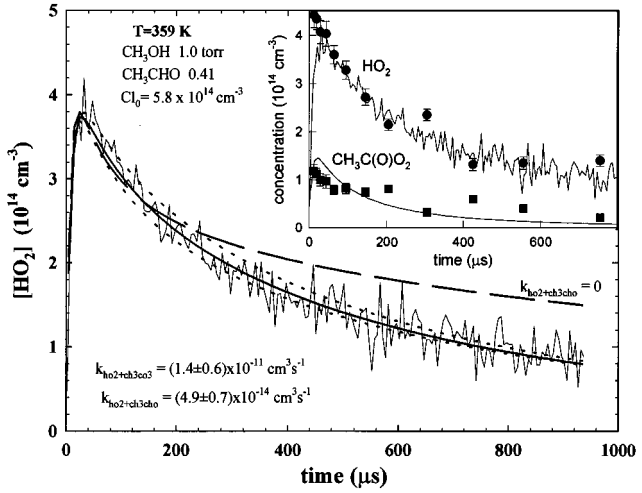

Figure 5. The HO_2 concentration in a $CH_3CHO/CH_3OH/Cl_2/O_2/N_2$ reaction mixture following 351 nm photolysis. The inset compares the HO_2 concentrations derived from deconvolution of the UV spectra (symbols) to those measured using IR probing (noisy line); also shown are the UV-based $CH_3C(O)O_2$ data. In the main figure, the solid line represents the best fit prediction from the model of Table 1, whereas the dotted lines show the limits imposed by the 2σ error bounds on k_1. The dashed line exhibits the best fit in the absence of a reaction between HO_2 and CH_3CHO.

$$HO_2 + CH_3CHO \rightarrow CH_3CH(OH)O_2 \qquad (13)$$

Including this reaction in the model (see Table 1) and allowing both k_1 and k_{13} to vary as fitting parameters lead to excellent fits of the IR measurements of $[HO_2]$, as illustrated by the solid line in Figure 5. Furthermore, the 1-hydroxy ethylperoxy radical generated by reaction 13 is expected, by analogy with $HOCH_2O_2$, to absorb UV radiation with a spectrum similar to that of CH_3O_2;[26] thus, a reaction between HO_2 and CH_3CHO could by this product contribute significantly to the anomalously high absorption in the CH_3O_2 spectral range. An accurate assessment of the contribution of the 1-hydroxy ethylperoxy radical to the UV absorbance spectra is not feasible since a reference spectrum of this radical is not available. Simply assuming it to be identical to that of methylperoxy leads to a total "CH_3O_2 + $CH_3CH(OH)O_2$" concentration that falls about halfway between the methylperoxy prediction and the "methylperoxy" data in Figure 4. The remaining discrepancy could easily arise from the fact that the CH_3O_2 and $CH_3CH(OH)O_2$ spectra are not identical and, therefore, that the deconvolution procedure of eq I incorrectly attempts to separate the overlapping contributions of six species into five components.

In principle, a "direct" measurement of reaction 13 should be feasible. Using the present technique, this would involve increasing the acetaldehyde concentration sufficiently to ensure that its reaction with HO_2 represents the dominant HO_2 loss mechanism and adjusting the methanol concentration to ensure that HO_2 radicals dominate over $CH_3C(O)O_2$ following Cl_2 photolysis. Unfortunately, this ideal situation is difficult to achieve in practice. The rapid reaction between chlorine atoms and acetaldehyde necessitates the use of high levels (10−20 Torr) of CH_3OH. Two difficulties are incurred: (1) the introduction of the methanol into the reaction cell; (2) the dependence of the HO_2 self-reaction on methanol concentration.[27] While not achieving ideal conditions, a number of experiments were performed at high initial acetaldehyde concentrations (~2 Torr) and with sufficient methanol to provide $[HO_2]_0/[CH_3C(O)O_2]_0$ ratios of 2−3.

Figure 6 demonstrates the results. Consistent with the example of Figure 5, a good fit of the data is obtained with a value of k_{13} that is commensurate with the rate constant for HO_2 + CH_2O.[26] In contrast, omitting reaction 13 and setting k_1 to the value of Moortgat et al.[9] severely underestimates the HO_2 decay

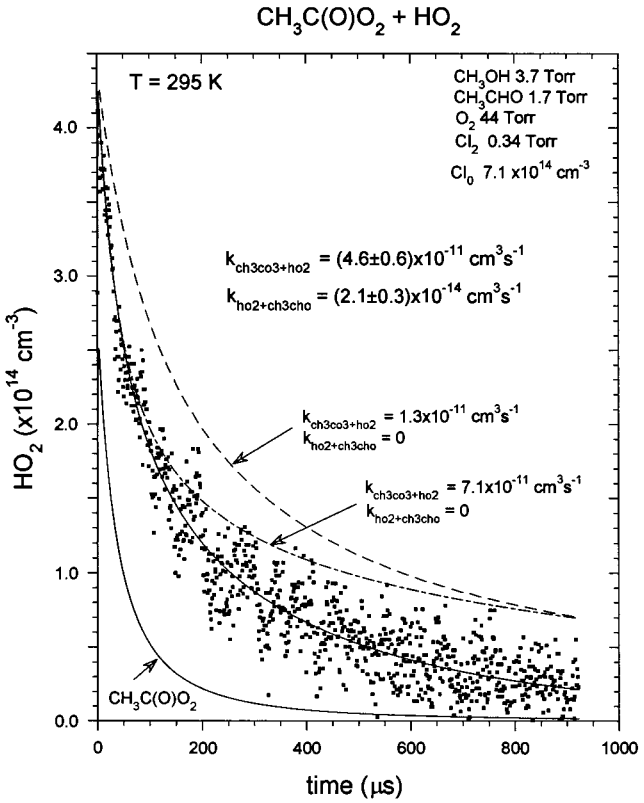

Figure 6. HO_2 concentration versus time at high $[CH_3CHO]_0$. The transient IR data are compared to the best fit prediction based on the present model, a prediction using the rate constant of Moortgat et al.,[9] and a fit to the present model assuming that $k_{13} = 0$. Predictions from a model modified to include $CH_3C(O)O_2$ regeneration via reaction 10 are indistinguishable from the best fit prediction.

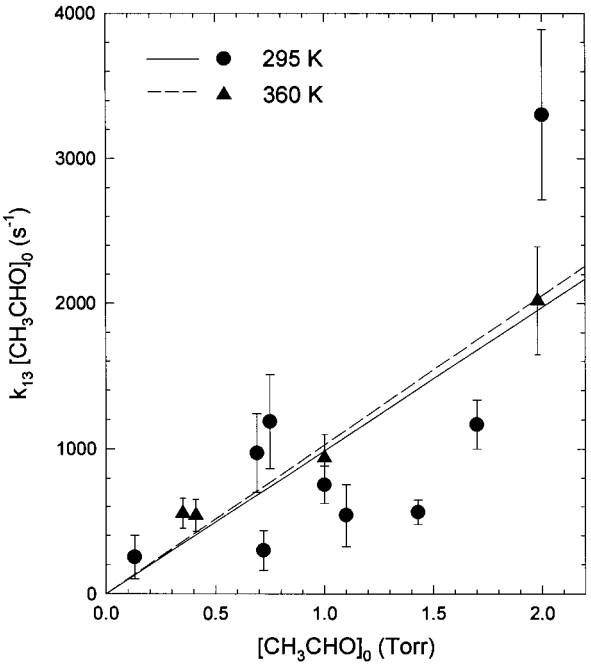

Figure 7. The variation in the $HO_2 + CH_3CHO$ reaction rate versus initial acetaldehyde concentration. Data are shown at two temperatures, 295 and 360 K.

rate (this remains the case regardless of the value used for the branching ratio of reaction 11). By substantially increasing k_1, the initial HO_2 loss can be modeled, but not the long-time behavior.

The variation in the rate for the $HO_2 + CH_3CHO$ reaction as a function of initial acetaldehyde concentration is demonstrated in Figure 7 at two temperatures. While they exhibit considerable scatter, the rates increase with increasing CH_3CHO level as would be expected for reaction 13. The determination of the error bars is described below; however, it is relevant to note that they include both statistical errors and systematic uncertainties, e.g., the initial total radical concentration. Yet the data scatter is outside the anticipated error bounds. A plausible explanation is as follows: the HO_2 absorbance is a weak signal recorded by the ac-coupled infrared detector out to relatively long times (~1 ms). We attempt to correct the natural tendency of the detector to decay to zero output, regardless of light level, by assuming an equivalent RC circuit; however, this is only an approximation. It is possible that this correction is inadequate and, furthermore, that it is affected by a detector baseline that is not always perfectly flat. Both affect the long-time appearance of the HO_2 decay, on which the value of k_{13} depends. In contrast, the fitting of k_1 is much less affected because, as shown in Figure 6, the acetylperoxy radicals are largely gone by 200 μs.

FTIR−smog chamber experiments provide further support for a hydroperoxy radical reaction with acetaldehyde. The evidence comes from a comparison of the Cl atom initiated loss of CH_3CHO relative to $^{13}CH_3OH$ in 700 Torr of N_2 versus air. If the hypothesis of a reaction between HO_2 and CH_3CHO holds true, then the loss of acetaldehyde relative to methanol should be higher in the air mixture as compared to the N_2 mixture, since reactions 4 and 5 lead to HO_2 formation in the presence of oxygen and this is not possible in the N_2 mixture. Typical gas mixtures used to test the hypothesis consisted of 31−51 mTorr of CH_3CHO, 2−218 mTorr of $^{13}CH_3OH$, and 200−500 mTorr of Cl_2, with $[^{13}CH_3OH]/[CH_3CHO]$ varied over the range 0.04−4.4. Isotopically labeled methanol is used as a precursor to distinguish it from CH_3OH formed as an oxidation product of acetaldehyde.

Figure 8A depicts the CH_3CHO loss compared to that of $^{13}CH_3OH$ in the N_2 buffer. The rate constant ratio deduced from a linear least-squares analysis of these data is $k_2/k_4 = 1.48 \pm 0.07$, independent of the $[CH_3OH]_0/[CH_3CHO]_0$ ratio. This result is in excellent agreement with the recent measurement of $k_2/k_4 = 1.50 \pm 0.10$ by Tyndall et al.,[18] who used mixtures of 35 mTorr of CH_3CHO and 9 mTorr of ^{13}CH3OH and found the ratio to be independent of total pressure of N_2 diluent over the 1−700 Torr range. It also compares well with the ratio of the recommended absolute rate constants, namely $k_2/k_4 = 7.2 \times 10^{-11}/5.3 \times 10^{-11} = 1.36 \pm 0.29$ (ref 28).

The situation is different when the experiments are carried out in air. In this case, rate constant ratios measured at a low $[^{13}CH_3OH]_0/[CH_3CHO]_0$ ratio are indistinguishable from those obtained in N_2. However, as evident in Figure 8B, increasing $[CH_3OH]_0/[CH_3CHO]_0$ produces a small but distinct deviation of k_2/k_4 from the values obtained in N_2 (indicated by the dotted line). A linear least-squares regression to the data obtained in air gives $k_2/k_4 = 1.89 \pm 0.10$, which is distinctly different from the value of $k_2/k_4 = 1.48 \pm 0.07$ in N_2. The ratio in air is higher, consistent with the existence of a second CH_3CHO removal pathway, and thus, supports the hypothesis of a reaction between HO_2 radicals and CH_3CHO.

The measured rate constants for the $CH_3C(O)O_2 + HO_2$ reaction are collected in Table 2 along with the values obtained for k_{13} , the initial radical concentrations, and the experimental conditions. The rate constants are determined from the best fit of the model in Table 1[20] to HO_2 concentration versus time traces recorded by transient IR absorption. The IR data were used because of the complications, discussed above, in decon-

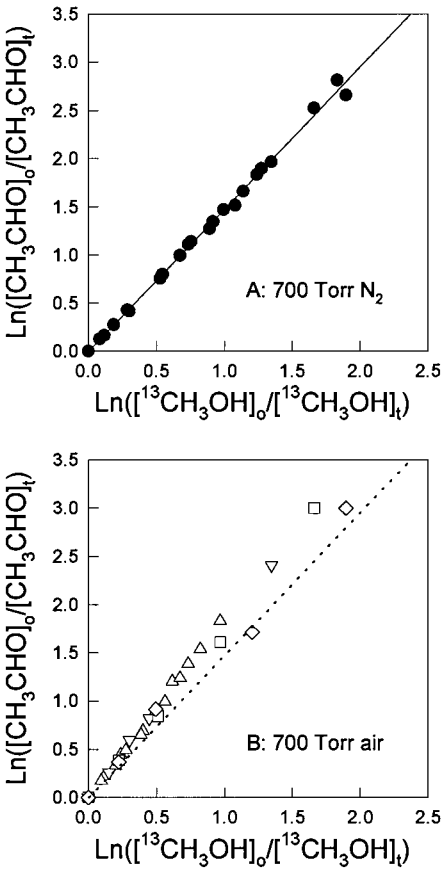

Figure 8. The loss of CH_3CHO versus $^{13}CH_3OH$ in 700 Torr of either (A) N_2 or (B) air diluent. Initial concentration ratios of $[^{13}CH_3OH]/[CH_3CHO]$ are 0.04−4.4 in the N_2 experiments and 0.04 (◇), 0.17 (□), 1.7 (△), and 2.4 (▽) for the experiments in air. The solid line in panel A is a linear least-squares fit of the data, which is reproduced as the dotted line in panel B.

voluting the time-resolved UV absorbances. As indicated in Table 2, however, both techniques were used under a subset of experimental conditions with generally good agreement found for the HO_2 concentrations, as illustrated in the inset to Figure 5.

Fitting the HO_2 concentration traces consists of the following steps. The total initial radical concentration is calibrated against the number of ethylperoxy radicals formed upon the substitution of ethane for acetaldehyde and methanol under otherwise identical experimental conditions. Where available, the UV absorbance data at early times, when HO_2 and $CH_3C(O)O_2$ contributions dominate, are used to partition of the initial radicals into $CH_3C(O)O_2$ and HO_2 populations; otherwise, this is based on the initial HO_2 concentration determined by the IR absorption. The model is then fit to the entire $[HO_2]$ versus time trace, using k_1 and k_{13} as fitting parameters and allowing small adjustments in the initial partitioning of radicals. Reactions of the $CH_3C(OH)HO_2$ product of reaction 13 with HO_2 and $CH_3C(O)O_2$ are included in the model by assuming the rate constants to be the same as those for the corresponding reactions with CH_3O_2. The effects of these reactions on the model predictions are small, less than indicated by the dashed error bars in Figure 5.

Several factors contribute to the error bars for k_1. These include signal-to-noise, uncertainties in the total number of radicals produced, and uncertainties in the rate constants of the principal reactions in the model, namely the HO_2 and $CH_3C(O)O_2$ self-reactions and the $HO_2 + CH_3CHO$ reaction. The fitting error, which includes the uncertainties in k_{13} and in the initial partitioning of radicals into HO_2 and $CH_3C(O)O_2$ populations, leads to the bulk of the error in k_1 , up to 25%. Including a 10% uncertainty in the total initial radical concentration contributes an additional 6% to the error. Uncertainties in the self-reaction rate constants of HO_2 and $CH_3C(O)O_2$ are smaller, adding about 1% each to the error. Combining these contributions statistically, the total 2σ error bars for k_1 are approximately ±25% in most cases.

Considerations for the error bars of k_{13} are similar. In this case, the fitting error, which includes the effects of uncertainties in k_1 and $[HO_2]_0/[CH_3C(O)O_2]_0$, varies more (10%−125%) and is the major source of error. At the lower end of this range, an additional 14% error contributed by uncertainty in total radical concentration and the 3% errors from uncertainties in the peroxy radical self-reaction rate constants add nonnegligible contributions to the overall error. As explained with reference to Figure 7, however, there are additional errors associated with the detector that we are unable to account for; thus, the fitted values of k_{13} fall into the range of $(1.2-6) \times 10^{-14}$ cm^3 s^{-1} at 295 K. For comparison, the literature rate constant for the analogous $HO_2 + HCHO$ reaction varies from 5.5×10^{-14} cm^3 s^{-1} at 360 K to 9.8×10^{-14} cm^3 s^{-1} at 270 K.[28] The values obtained here for k_{13} are of the same order.

In contrast to k_{13}, the $HO_2 + CH_3C(O)O_2$ rate constant remains essentially unaffected by changes in $[CH_3CHO]_0$ and variation of $[HO_2]_0/[CH_3C(O)O_2]_0$ between 0.7 and 3.0 (see Table 2). The data displayed in Figure 9 indicate consistent values for this rate constant at each temperature (with one outlier at 359 K; Table 2). The temperature dependence of the $CH_3C(O)O_2 + HO_2$ rate constant follows the Arrhenius expression

$$k_1 = (3.9^{+5.0}_{-2.3}) \times 10^{-13} e^{(1350\pm250)/T} \text{ cm}^3 \text{ s}^{-1} \qquad \text{(III)}$$

The negative temperature dependence is typical of $HO_2 + RO_2$ reactions and suggests that the reaction proceeds through a rate-limiting adduct formation.

B. Product Studies. *Reactions of Cl Atoms with $CH_3C(O)OH$ and $CH_3C(O)OOH$.* Prior to investigating the products arising from the reaction of $CH_3C(O)O_2$ and HO_2 radicals, relative rate experiments were performed using the FTIR system to investigate the kinetics of the reaction of Cl atoms with $CH_3C(O)OH$ and $CH_3C(O)OOH$. The relative rate technique is described in detail elsewhere.[29,30] Photolysis of molecular chlorine provides the source of Cl atoms. The kinetics of reaction 14 are measured relative to reaction 16, while reaction 15 was measured relative to reactions 17 and 18.

$$Cl + CH_3C(O)OH \rightarrow \text{products} \qquad (14)$$

$$Cl + CH_3C(O)OOH \rightarrow \text{products} \qquad (15)$$

$$Cl + CH_4 \rightarrow HCl + CH_3 \qquad (16)$$

$$Cl + CD_4 \rightarrow DCl + CD_3 \qquad (17)$$

$$Cl + \text{HCFC-141b} \rightarrow \text{products} \qquad (18)$$

To test for a loss of reactants via photolysis or heterogeneous reactions, mixtures of $CH_3C(O)OH$ and $CH_3C(O)OOH$ in air were prepared without Cl_2, left to stand in the dark for 10 min, and then irradiated for 10 min. There was no loss (<2%) of either compound, showing that photolysis and heterogeneous loss are insignificant.

TABLE 2: $CH_3C(O)O_2 + HO_2$ Rate Constants

conditions								results[a]	
temp (K)	P_{tot} (Torr)	O_2 (Torr)	Cl_2 (Torr)	CH_3CHO (Torr)	CH_3OH (Torr)	$[HO_2]_0$ (10^{14} cm^{-3})	$[CH_3C(O)O_2]_0$ (10^{14} cm^{-3})	$k_{HO_2+CH_3CHO}$ (10^{-14} cm^{-3} s^{-1})	$k_{CH_3CO_3+HO_2}$ (10^{-1} cm^{-3} s^{-1})
269[b]	50.2	40.6	0.37	0.60	1.27	4.0	1.6	20 ± 3	5.9 ± 2.6
269	50.3	40.8	0.36	0.70	1.25	3.9	2.8	8.0 ± 1.4	5.1 ± 1.3
269	50.7	16.2	0.44	0.80	.90	4.2	3.3	16 ± 3	4.8 ± 1.4
297[b]	51.3	26.2	0.40	0.69	1.56	4.7	2.0	4.3 ± 1.2	4.4 ± 1.6
293	50.2	15.2	0.53	0.75	.90	5.3	3.8	4.8 ± 1.3	4.0 ± 0.9
295	52.0	22.8	0.42	0.13	0.16	5.6	1.8	5.9 ± 3.5	4.9 ± 1.5
295	54.3	23.2	0.41	1.10	1.38	4.2	3.4	1.5 ± 0.6	3.2 ± 0.9
295[b]	48.8	14.9	0.51	0.72	0.88	4.5	3.5	1.3 ± 0.6	3.3 ± 0.7
295	57.0	45.2	0.34	0.97	3.77	6.3	2.1	2.3 ± 0.4	4.0 ± 0.6
295	61.0	48.3	0.35	1.43	4.03	5.4	2.5	1.2 ± 0.3	4.7 ± 0.8
295	56.9	44.8	0.34	1.68	3.70	5.5	2.6	2.1 ± 0.3	4.6 ± 0.7
295	56.0	45.2	0.34	2.04	3.77	4.9	3.5	5.0 ± 0.9	3.6 ± 0.7
325[b]	50.5	25.3	0.40	0.66	1.50	4.8	1.8	4.6 ± 0.9	2.5 ± 0.9
328	50.4	42.8	0.30	0.63	2.25	2.5	2.4	7.4 ± 2.2	2.3 ± 0.6
329[b]	50.1	41.7	0.32	0.33	1.28	3.8	1.2	2.8 ± 0.7	2.1 ± 0.6
359[b]	54.3	43.7	0.44	0.41	1.02	3.7	1.5	4.9 ± 1.0	1.4 ± 0.6
359	50.7	41.2	0.42	0.35	0.39	3.7	2.8	5.9 ± 1.1	1.8 ± 0.3
359	50.8	39.9	0.42	1.00	1.14	3.1	3.4	3.5 ± 0.6	1.3 ± 0.2
359	50.9	37.9	0.42	1.98	2.25	2.9	4.0	3.8 ± 0.7	0.6 ± 0.2
363	51.0	43.2	0.31	0.74	0.65	1.9	2.9	2.1 ± 2.6	2.0 ± 0.6

[a] Error bars are $\pm 2\sigma$ and include fitting and systematic uncertainties. [b] Indicates that a UV experiment was done under the same conditions.

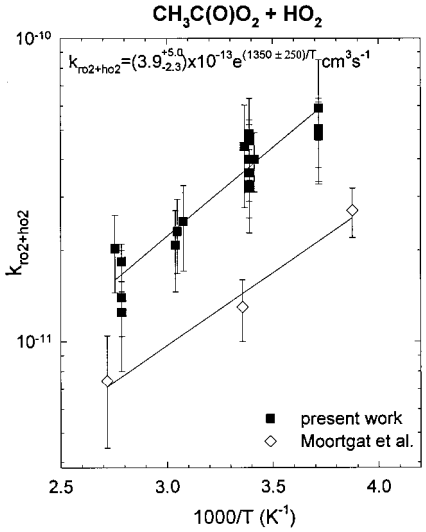

Figure 9. Temperature dependence of the $CH_3C(O)O_2 + HO_2$ rate constant. The solid lines represent least-squares fits of the rate constants to the Arrhenius expression.

Figure 10A shows the observed loss of $CH_3C(O)OH$ versus that of CH_4 following UV irradiation of a $CH_3C(O)OH/CH_4/Cl_2$ mixture in 700 Torr total pressure of N_2. Figure 10B shows $CH_3C(O)OOH$ loss versus those of CD_4 and $CFCl_2CH_3$ upon the UV irradiation of $CH_3C(O)OOH/CD_4/Cl_2$ and $CH_3C(O)OOH/CFCl_2CH_3/Cl_2$ mixtures in 700 Torr total pressure of N_2. Linear least-squares analyses of these data give $k_{14}/k_{16} = 0.25 \pm 0.03$, $k_{15}/k_{17} = 0.81 \pm 0.06$, and $k_{15}/k_{18} = 2.06 \pm 0.24$. Inserting the literature values $k_{16} = 1.0 \times 10^{-13}$ [ref 15], $k_{17} = 6.1 \times 10^{-15}$ [ref 30], and $k_{18} = 2.0 \times 10^{-15}$ cm^3 s^{-1} [ref 30] yields $k_{14} = (2.5 \pm 0.3) \times 10^{-14}$, $k_{15} = (4.9 \pm 0.6) \times 10^{-15}$, and $k_{15} = (4.1 \pm 0.5) \times 10^{-15}$ cm^3 s^{-1}, respectively. Unless otherwise noted, errors quoted for relative rates are 2σ based on the scatter in the data. When these are converted to rate constants via comparison to the reference reaction, the uncertainty in the latter quantity is also incorporated into the overall error. There being no inherent reason to prefer one reference reaction over the other, we take for k_{15} the average of the two relative rate determinations and set the error limits to encompass the extremes

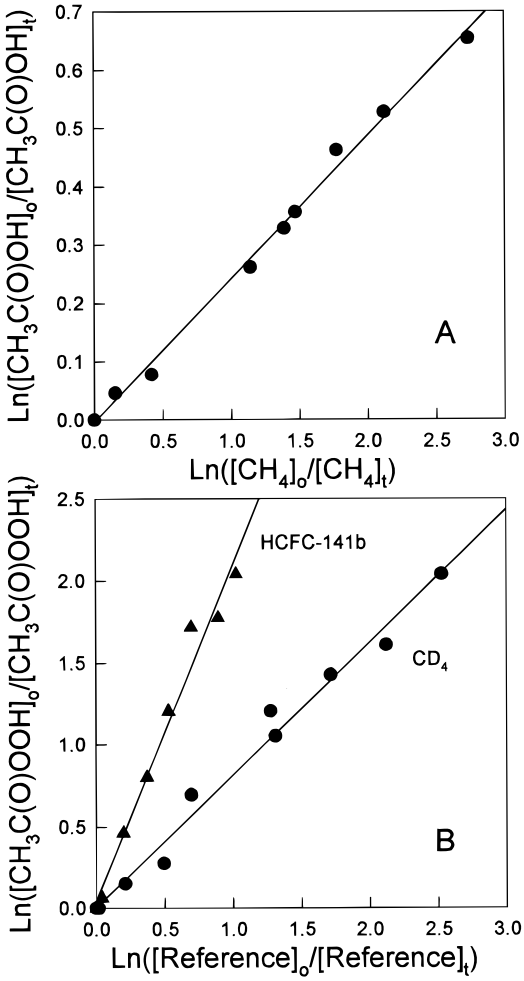

Figure 10. Plots of the loss of $CH_3C(O)OH$ versus CH_4 and the loss of $CH_3C(O)OOH$ versus HCFC-141b ($CFCl_2CH_3$) and CD_4 when mixtures containing these compounds are exposed to Cl atoms in 700 Torr of N_2 diluent at 296 K. Solid lines are linear least-squares fits.

of the individual determinations; hence, $k_{15} = (4.5 \pm 1.0) \times 10^{-15}$ cm^3 s^{-1}. Our measurement of $k_{14} = (2.5 \pm 0.3) \times 10^{-14}$ cm^3 s^{-1} agrees well with the previous determination of $k_{14} =$

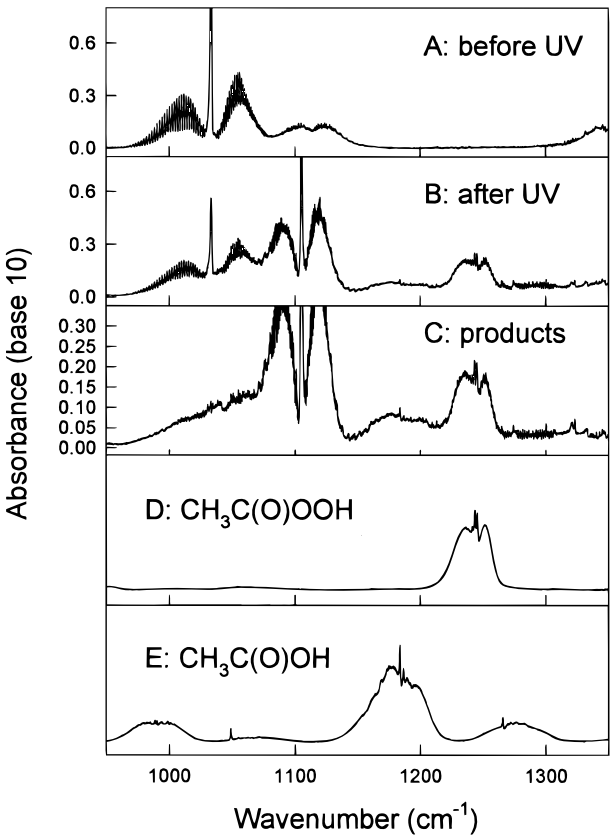

Figure 11. IR spectra acquired before (A) and after (B) 2 min irradiation of a mixture containing 52.1 mTorr of CH_3CHO, 26.1 mTorr of CH_3OH, and 290 mTorr of Cl_2 in 700 Torr of air diluent. Subtraction of IR features attributable to CH_3CHO and CH_3OH gives the product spectrum shown in panel C (note the change in *y*-axis scale). Reference spectra of $CH_3C(O)OOH$ and $CH_3C(O)OH$ are shown in panels D and E.

2.8×10^{-14} cm^3 s^{-1} by Koch and Moortgat[31]. There are no literature values against which to compare our measurement of k_{15}.

Product Study of the $CH_3C(O)O_2 + HO_2$ Reaction. The products of reaction 1 were studied using the FTIR−smog chamber system and UV irradiation of $CH_3CHO/CH_3OH/Cl_2$/air mixtures. Atomic chlorine formed by the photolysis of molecular chlorine is converted into $CH_3C(O)O_2$ and HO_2 radicals via reactions 2−5. The acetylperoxy self-reaction (7), its reaction with HO_2 (1), and its reaction with CH_3O_2 (11) then compete for the available $CH_3C(O)O_2$ radicals. The experimental approach to ascertain the branching ratio of reaction 1 is to measure $CH_3C(O)OOH$ and $CH_3C(O)OH$ yields as a function of the initial concentration ratio, $[CH_3OH]_0/[CH_3CHO]_0$. As this ratio increases, so does the $[HO_2]/[CH_3C(O)O_2]$ ratio. Reaction 1 thereby becomes a more important $CH_3C(O)O_2$ loss pathway relative to reactions 7 and 11, and at sufficiently high ratios, it becomes essentially the sole loss mechanism. Increasing $[CH_3OH]_0/[CH_3CHO]_0$ beyond this point will not change the observed $CH_3C(O)OOH$ and $CH_3C(O)OH$ yields; thus, this asymptotic regime reflects the relative importance of channels 1a and 1b.

Both $CH_3C(O)OOH$ and $CH_3C(O)OH$ are observed as products following the UV irradiation of $CH_3CHO/CH_3OH/Cl_2$/air mixtures. Figure 11 compares spectra acquired before (A) and after (B) a 2 min irradiation of a mixture of 52.1 mTorr of CH_3CHO, 26.1 mTorr of CH_3OH, and 290 mTorr of Cl_2 in 700 Torr of air diluent. Subtraction of IR features attributable to the CH_3CHO and CH_3OH reactants gives the product spectrum shown in panel C. The large feature at 1104 cm^{-1} arises from HCOOH, which is a well-established photooxidation product of CH_3OH. The loss of CH_3CHO is 42.7 mTorr. Comparison with the reference spectra of $CH_3C(O)OOH$ and $CH_3C(O)OH$, shown in parts D and E of Figure 11, confirms the species identification. Figure 12 depicts the observed formation of $CH_3C(O)OOH$ and $CH_3C(O)OH$ versus the loss of CH_3CHO in this experiment.

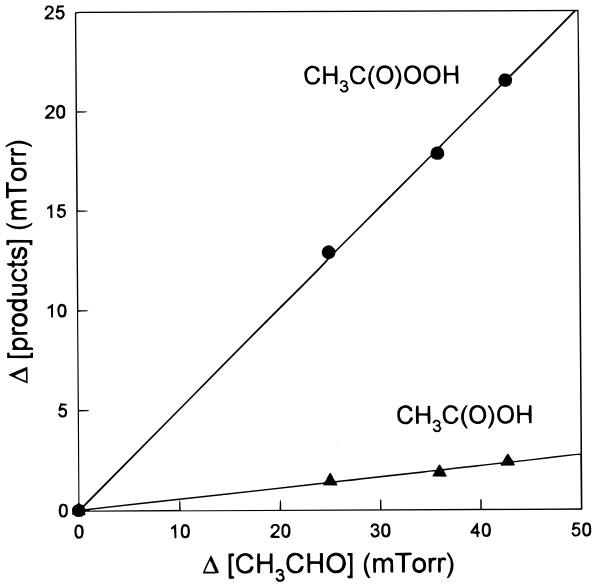

Figure 12. The formation of $CH_3C(O)OOH$ and $CH_3C(O)OH$ versus CH_3CHO loss following UV irradiation of a mixture of 52.1 mTorr of CH_3CHO, 26.1 mTorr of CH_3OH, and 290 mTorr of Cl_2 in 700 Torr of air diluent.

As with all product studies, the possibility of product loss via secondary reactions deserves careful attention. Potential unwanted secondary processes include photolysis, heterogeneous losses, and reaction with Cl atoms. As discussed above, no discernible photolytic or heterogeneous loss of $CH_3C(O)OOH$ or $CH_3C(O)OH$ was detected over the time scale of the present experiments. Furthermore, considering that $CH_3C(O)OH$ and $CH_3C(O)OOH$ are, respectively, 3000 and 16000 times less reactive toward Cl atoms than is CH_3CHO, their loss via Cl atom attack is insignificant.

The observed yields of $CH_3C(O)OOH$ and $CH_3C(O)OH$ are plotted versus $[CH_3OH]_0/[CH_3CHO]_0$ in Figure 13. This figure demonstrates that increasing the initial concentration ratio from 0 to 2 raises both the $CH_3C(O)OOH$ and $CH_3C(O)OH$ yields, as expected from an increased importance of reaction 1 relative to reactions 7 and 11. Both product yields reach plateaus for $[CH_3OH]_0/[CH_3CHO]_0 > 2$, indicating that the $CH_3C(O)O_2$ loss occurs almost entirely via reaction 1. Averaging the product levels in this regime provides a $CH_3C(O)OOH$ yield of (75 ± 6)% and a $CH_3C(O)OH$ yield of (8.5 ± 0.9)%, including 2σ fitting errors. We estimate that potential systematic uncertainties in quantifying the $CH_3C(O)OOH$ and $CH_3C(O)OH$ yields are 20% and 15%, respectively. Using conventional error propagation to incorporate these uncertainties leads to yields for $CH_3C(O)OOH$ and $CH_3C(O)OH$ of (75 ± 16)% and (8.5 ± 1.6)%, respectively. Together, $CH_3C(O)OOH$ and $CH_3C(O)OH$ account for (84 ± 17)% of the loss of CH_3CHO.

There are two factors that account for a carbon balance of less than 100%. First, although reaction 1 dominates the loss of $CH_3C(O)O_2$ radicals under conditions where $[CH_3OH]_0/[CH_3CHO]_0 > 2$, a small loss of $CH_3C(O)O_2$ radicals via self-reaction and reaction with CH_3O_2 is unavoidable. Second, as discussed

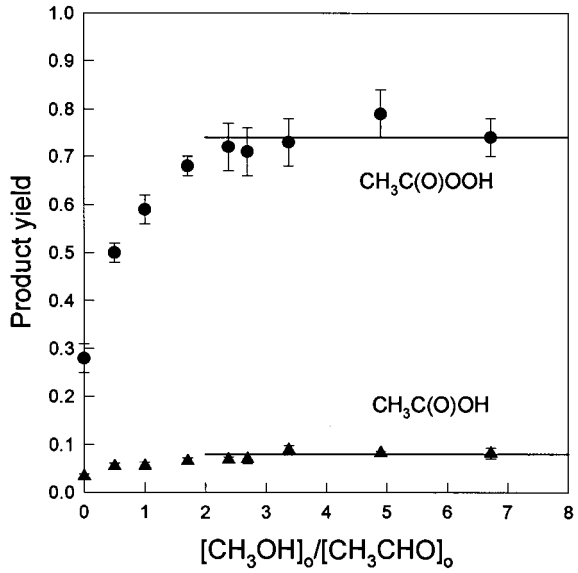

Figure 13. Observed molar product yields for $CH_3C(O)OOH$ and $CH_3C(O)OH$ versus the initial concentration ratio $[CH_3OH]_0/[CH_3CHO]_0$ following the UV irradiation of $CH_3CHO/CH_3OH/Cl_2$/air mixtures at 700 Torr total pressure at 296 K. The lines are averages of the data for $[CH_3OH]_0/[CH_3CHO]_0 > 2$.

in Section III.A, we have evidence that some CH_3CHO is removed via reaction with HO_2 , presumably producing $CH_3C(OH)HO_2$ radicals. By analogy to $C_2H_5O_2$ radicals,[32] we expect that they will react with HO_2 to give the corresponding hydroperoxide; thus, it is unlikely that $CH_3C(OH)HO_2$ is converted into either peracetic or acetic acid under our experimental conditions. An estimate of the magnitude of CH_3CHO loss via reaction with HO_2 can be derived from the data shown in Figure 8. Linear least-squares analysis of the data in Figure 8B, using $[CH_3OH]_0/[CH_3CHO]_0 = 2.4$, gives an apparent value of $k_2/k_4 = 1.8$, which is 20% greater than the "true" value of $k_2/k_4 = 1.48 \pm 0.07$ obtained from Figure 8A. Thus, for the experiment with $[CH_3OH]_o/[CH_3CHO]_o = 2.4$, the CH_3CHO loss is approximately 20% greater than can be explained solely on the basis of Cl atom chemistry. This additional loss of CH_3CHO is of the correct magnitude to explain why the combined $CH_3C(O)OOH$ and $CH_3C(O)OH$ yield of (84 ± 17)% does not account for 100% of the acetaldehyde loss.

Figure 14 shows the observed formation of $CH_3C(O)OOH$ versus that of $CH_3C(O)OH$ following UV irradiation of $CH_3CHO/CH_3OH/Cl_2$/air mixtures. Results from experiments with $[CH_3OH]_0/[CH_3CHO]_0 > 2$ are indicated by the filled symbols, while those with $[CH_3OH]_0/[CH_3CHO]_0 < 2$ are indicated by open symbols. There is no discernible impact of the $[CH_3OH]_0/[CH_3CHO]_0$ ratio on the relative yields of $CH_3C(O)OOH$ and $CH_3C(O)OH$, suggesting that reaction 1 is the dominant source of both acids. Assuming that $CH_3C(O)OOH$ and $CH_3C(O)OH$ are formed solely via reaction 1, a linear least-squares analysis of the data in Figure 14 gives $k_{1a}/(k_{1a}+k_{1b}) = 0.90 \pm 0.02$ and $k_{1b}/(k_{1a}+k_{1b}) = 0.10 \pm 0.02$.

As reported by Niki et al.[8] and Horie and Moortgat,[10] ozone is formed as a coproduct with $CH_3C(O)OH$ in channel 1b. Unfortunately, the IR spectrum of ozone is overlapped by that of CH_3OH, so it is not possible to confirm the formation of O_3 in the experiments using $CH_3CHO/CH_3OH/Cl_2$/air mixtures described above. An additional set of experiments was conducted using mixtures of 73−228 mTorr of CH_3CHO and 0.3−0.4 Torr of Cl_2 in 700 Torr of air to quantify ozone formation. Figure 15 shows the yields of $CH_3C(O)OOH$, $CH_3C(O)OH$, and

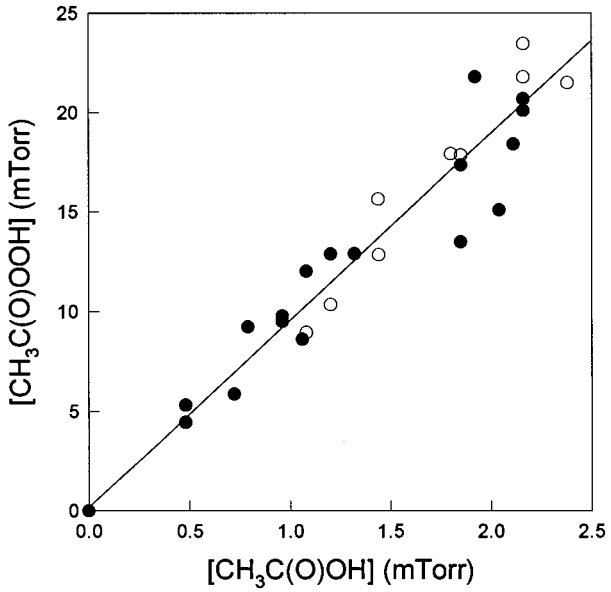

Figure 14. The formation of $CH_3C(O)OOH$ versus that of $CH_3C(O)OH$ following the irradiation of $CH_3CHO/CH_3OH/Cl_2$/air mixtures with $[CH_3OH]_0/[CH_3CHO]_0 > 2$ (filled symbols) and $[CH_3OH]_0/[CH_3CHO]_0 < 2$ (open symbols). The solid line is a linear least-squares fit that has a slope of 9.2 ± 0.7.

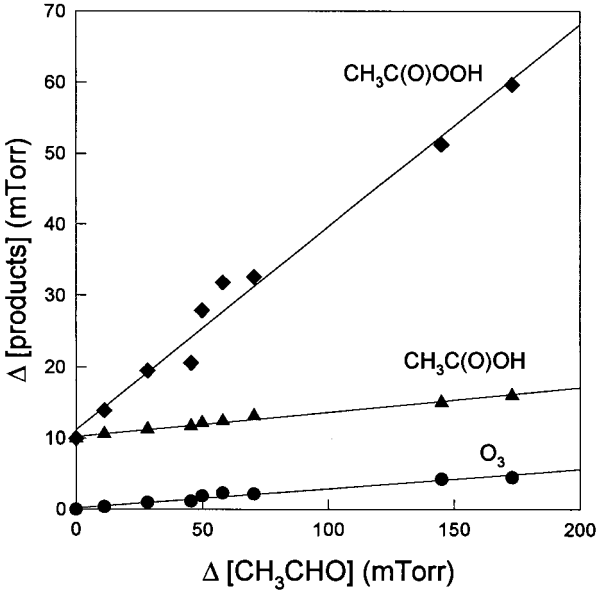

Figure 15. Observed formation of $CH_3C(O)OOH$ (◆), $CH_3C(O)OH$ (▲), and O_3 (●) versus loss of CH_3CHO following irradiation of CH_3CHO/Cl_2/air mixtures. For clarity, the data for $CH_3C(O)OOH$ and $CH_3C(O)OH$ have been shifted vertically by 10 units.

O_3. A correction is necessary to account for the loss of ozone via

$$Cl + O_3 \rightarrow ClO + O_2 \qquad (19)$$

This is computed using the Acuchem program with $k_2 = 7.2 \times 10^{-11}$ cm^3 s^{-1} and $k_{19} = 1.2 \times 10^{-11}$ cm^3 s^{-1} [ref 15]. The corrections are in the range 1−17% and have been applied to the ozone data in Figure 15. The ClO radicals react with the various peroxy radicals in the system and represent a minor loss pathway for these species.

A linear least-squares analysis of the data in Figure 15 provides yields of 0.28 ± 0.03 for $CH_3C(O)OOH$, 0.034 ± 0.005 for $CH_3C(O)OH$, and 0.027 ± 0.004 for O_3. Within the

TABLE 3: Ozone Channel Branching Fraction

temp (K)	P_{tot} (Torr)	O_2 (Torr)	Cl_2 (Torr)	CH_3CHO (Torr)	CH_3OH (Torr)	$[HO_2]_0$ (10^{14} cm^{-3})	$[CH_3C(O)O_2]_0$ (10^{14} cm^{-3})	$[O_3]$ yield (10^{-14} cm^3 s^{-1})	k_{1b}/k_1[a]
265	132	30.8	0.33	0.98	1.07	3.7	4.6	0.63	0.21 ± 0.04
266	50.5	23.8	0.41	0.67	2.91	4.3	3.1	0.47	0.20 ± 0.04
269	50.2	40.6	0.37	0.60	1.27	3.1	2.0	0.29	0.15 ± 0.05
297	51.3	26.2	0.40	0.69	1.56	5.2	2.4	0.35	0.18 ± 0.04
295	132	29.0	0.31	1.17	1.11	4.5	4.1	0.40	0.16 ± 0.04
295	48.8	14.9	0.51	0.72	0.88	3.6	4.2	0.35	0.14 ± 0.03
325	50.5	25.3	0.40	0.66	1.50	4.6	1.6	0.20	0.15 ± 0.05
329	50.1	41.7	0.32	0.33	1.28	4.7	0.80	0.11	0.11 ± 0.05
359	54.3	43.7	0.44	0.41	1.04	4.6	1.3	0.14	0.13 ± 0.07

[a] Error bars are $\pm 2\sigma$.

experimental uncertainties, O_3 formation is indistinguishable from that of $CH_3C(O)OH$. It should be noted that no correction has been made for O_3 loss via its reaction with HO_2 radicals, although given the similarity between the O_3 and $CH_3C(O)OH$ yields, this reaction appears to be of minor importance.

The flash photolysis/time-resolved UV spectroscopy experiments provide additional data on the branching fraction for reaction 1. Of the six species that contribute to the absorbance of the reaction mixture, the five shown in Figure 1 and the 1-hydroxy ethylperoxy product of reaction 13, only two remain in the reaction cell at long times, namely ozone and "products". The others are lost via the reactions in Table 1. Judging from Figure 1, it is easy to separate the contributions of these two components from the absorbance spectra at long time and, thereby, obtain an ozone yield. This yield cannot be used directly to compute the branching fraction for reaction 1 since, unlike with the FTIR−smog chamber system, $CH_3C(O)O_2$ removal via self-reaction and reaction with CH_3O_2 remains competitive with reaction 1, owing to the much higher radical concentrations relevant to the flash photolysis experiments.

The branching can be deduced by comparing the ozone yield to predictions based on the kinetic model of Table 1 along with the values of k_1 and k_{13} listed in Table 2. An example of a fit to ozone data is provided in Figure 4. The results of such comparisons are presented in Table 3 along with the pertinent experimental conditions and are illustrated by Figure 16. The average value of $k_{1b}/k = 0.16 \pm 0.04$ at 295 K is somewhat larger than the result of $k_{1b}/k = 0.10 \pm 0.02$ obtained from the smog chamber experiments. Because of the complexity of the reaction model used to extract the ozone branching fraction from the kinetic data, this level of agreement should be considered reasonable. A weighted average of $k_{1b}/k = 0.12 \pm 0.04$ is consistent with both sets of experiments. It appears from Figure 16 that the branching for the ozone channel has a slight negative temperature dependence; however, a quantitative determination of this effect is not warranted owing to the scatter in the data.

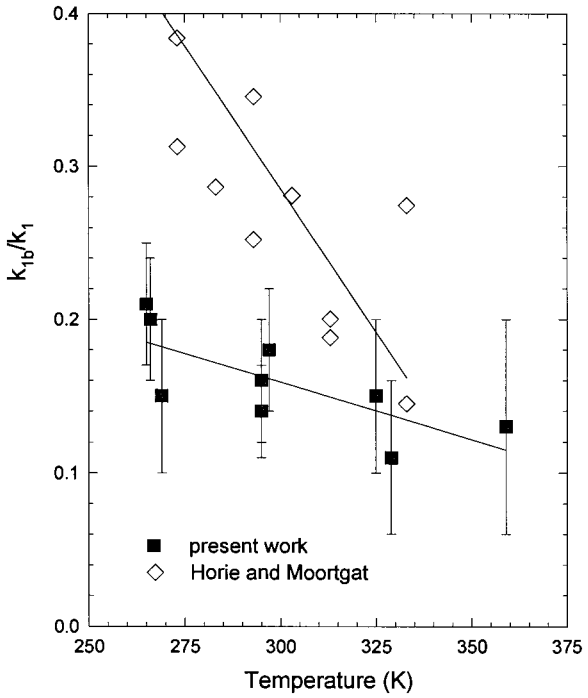

Figure 16. Temperature dependence of the branching fraction for reaction 1 to produce acetic acid and ozone. The solid lines represent linear regressions.

IV. Discussion

Rate constants for the reaction of HO_2 with $CH_3C(O)O_2$ have been reported previously by Moortgat et al.[9] A comparison of their values with the present results is presented in Figure 9. Moortgat et al. used flash photolysis/UV absorption to measure the rate constants and generated the peroxy radicals via reactions 2−5 from methanol and acetaldehyde precursors. Two important differences exist, however, between their study and ours. First, they made absorbance measurements at only a few fixed wavelengths in contrast to the full spectra recorded in the present study. Second, transient IR absorption is employed in the present study to confirm the HO_2 decay and determine k_1.

The comparison in Figure 9 shows our value of k_1 to be larger than the previous determination by a factor ranging from 2.8 at 260 K to 2.1 at 360 K, as determined from the ratio of the respective least-squares regressions. The "true" discrepancy is actually about 25% larger than this because the "best" HO_2 and $CH_3C(O)O_2$ UV cross sections available to Moortgat et al.[9] were about 25% larger than the currently accepted values. On the basis of the difficulties that we encountered in separating the contributions of the various UV absorbing species present in this reaction system, even when full spectra are recorded, we suspect that the reliance on fixed single wavelength absorption measurements in the earlier work is, at least partly, the cause of the disagreement in rate constant values.

The difficulties inherent in the fixed wavelength approach are illustrated by Figure 17. Here, the symbols represent absorbance versus time slices taken at three wavelengths from the full spectral surface in Figure 3. Solid lines show the predictions from the model of Table 1, whereas dashed lines give the predictions based on the smaller value of k_1 reported by Moortgat et al.[9] and with no reaction between HO_2 and acetaldehyde. The absorbances are calculated from the predicted concentrations of HO_2 , $CH_3C(O)O_2$, CH_3O_2 , and O_3 , using the currently recommended UV cross sections.[14] The absorbance data at these three wavelengths seem to be fit better when using the rate constant reported by Moortgat et al.[9] as compared to

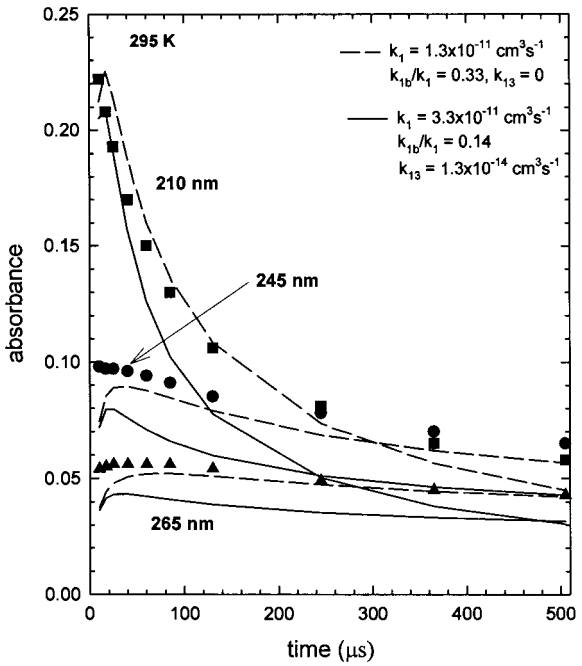

Figure 17. Comparison of predicted and measured values of the total UV absorbance at three fixed wavelengths. Solid lines represent predictions of the absorbance from the present model *based solely on the HO_2, $CH_3C(O)O_2$, CH_3O_2, and O_3 contributions.* Dashed lines represent predictions based on the value of k_1 reported by Moortgat et al.,[9] with $k_{13} = 0$ and $k_{1b}/k_1 = 0.33$.

the presently measured value. However, when the full spectra are deconvoluted, as in Figure 4, the situation is reversed and our value of k_1 gives a superior fit to the HO_2 concentration. Furthermore, the present determination of k_1 fits the IR measurements of HO_2 concentrations, as shown in Figures 5 and 6. The principal reason for the reversal in quality of fit between the absorbance data in Figure 17 and the concentration data in Figures 4, 5, and 6 is that, when relying simply on absorbances at a limited number of wavelengths, there is no indication that the "apparent" methylperoxy contribution is anomalously high. The contribution from $CH_3C(OH)HO_2$, which is expected to have a UV spectrum similar to that of CH_3O_2, is not accounted for; instead, it is compensated for by the lower value of k_1 . Likewise, the contribution by the "products" to the overall absorbance was ignored in calculating the dashed lines in Figure 17, and this, too, affects what value of k_1 gives the best fit to the absorbance data.

The preceding example is meant as an illustration of potential problems encountered when using fixed wavelengths to analyze a complex absorbing reaction mixture and not as a reanalysis of the data of Moortgat et al.[9] It shows that our UV absorption data are consistent with that of Moortgat et al.; if we were to employ the analysis at fixed wavelengths used by them, we would arrive at essentially the same value of k_1 that they did. However, our IR measurements of HO_2 (Figures 5 and 6) and those based on deconvolution of the UV data (Figure 4) show it to decay substantially faster than can be accounted for by the value of k_1 reported by Moortgat et al.[9] In the absence of the postulated reaction between HO_2 and acetaldehyde, a rate constant roughly 5 times larger becomes necessary to describe at least the initial HO_2 decay. We believe that our kinetics measurements made as a function of $[CH_3CHO]_0$ and the smog chamber observations of a higher rate of CH_3CHO loss relative to CH_3OH in air versus N_2, while not conclusive, are sufficient to support the hypothesis of a reaction between HO_2 radicals and acetaldehyde. Therefore, we include this reaction in our fitting procedure and report the values for k_1 listed in Table 2 and shown in Figure 9.

The branching of reaction 1 into peracetic acid and acetic acid plus ozone channels has been investigated previously at 295 K by three groups, all of which report values of k_{1b}/k_1 2−3 times larger than those found here. Niki et al.,[8] using a FTIR−smog chamber system, reported $k_{1b}/k_1 = 0.25 \pm 0.05$. By varying the ozone contribution to the total UV absorbance at 210, 245, and 265 nm, Moortgat et al.[9] obtained $k_{1b}/k_1 = 0.33 \pm 0.07$, independent of temperature. Finally, Horie and Moortgat[10] derive a ratio of $k_{1b}/k_1 = 0.28 \pm 0.05$ from experiments involving the photolysis of biacetyl. In contrast, the FTIR−smog chamber and UV absorbance experiments reported here give ratios of $k_{1b}/k_1 = 0.10 \pm 0.02$ and 0.16 ± 0.04, respectively. It is also worth noting (Figure 16) that the branching fraction of Horie and Moortgat[10] exhibits a significantly stronger temperature dependence than that found in the present study.

It is unclear why our determination of the branching fraction differs from that of Niki et al.[8] The discrepancy between the present ratio and that of Moortgat et al.[9] probably exists for the same reasons as discussed above with regard to k_1. Horie and Moortgat[10] derived the branching ratio for reaction 1 from the ratio of the peracetic acid to ozone yield recorded from the photolysis of biacetyl. This differs from the present determination in two ways. First, they sampled their products from a flowing reaction mixture and analyzed the product yields by matrix-isolated IR absorption, whereas the present experiments relied on in situ measurements. Thus, it is possible that the relative amounts of peracetic acid to ozone were affected by the sampling. Second, they relied on the photooxidation of biacetyl to produce HO_2, whereas in the present study, the HO_2 to $CH_3C(O)O_2$ ratio is varied by changing the relative concentrations of the methanol and acetaldehyde precursors. As discussed in Section III.B, this is important because of the complex secondary chemistry involved.

A simple estimate can be made regarding the atmospheric importance of a reaction between hydroperoxy radicals and acetaldehyde. The major atmospheric removal mechanism for acetaldehyde is expected to be via hydrogen abstraction by OH radicals, which proceeds with a rate constant of 1.4×10^{-11} cm^3 s^{-1} at 295 K.[15] Except under unusual circumstances, the reaction with HO_2 is not expected to change this. Whereas the tropospheric HO_2 concentrations can exceed those of OH (which range[33] from 0.4 to 9×10^6 cm^{-3}) by 2 orders of magnitude, the rate constant for acetaldehyde removal by HO_2 is approximately 500 times smaller than that for its loss via reaction with OH. Thus, the HO_2 reaction should represent a minor removal pathway for acetaldehyde, and the $CH_3C(OH)HO_2$ radical should be a minor degradation product. Since the reactions with OH and HO_2 both exhibit negative temperature dependences, this would remain the case as a function of temperature and, hence, altitude.

The rate constant for the $HO_2 + CH_3C(O)O_2$ reaction differs considerably from the version employed by Stockwell et al.[6] to model atmospheric PAN concentrations. In their second generation regional acid deposition mechanism[34] (RADM), these authors take the expression $7.7 \times 10^{-14}e^{1300/T}$ cm^3 s^{-1} to describe the kinetics of reaction 1. Interestingly, the temperature dependence coincides very closely with our measurement. However, the magnitudes of the rate constants reported here are over 5 times larger than those used in their RADM. This is not the only acetylperoxy reaction for which newly measured rate constants differ from those employed by Stockwell et al.[34] Recent data for the competing reaction with NO give rate

constants about twice as large as used in their model,[13,35,36] whereas a recent investigation of the acetylperoxy self-reaction leads to a significantly stronger temperature dependence and rate constants ranging from 5 to 8 times larger than those in the RADM.[34] How these changes affect model predictions of the nighttime PAN decomposition relative to ozone loss awaits detailed calculations that are beyond the scope of the present paper. However, the increased reactivity of the acetylperoxy radical with HO_2 and other peroxy radicals that has been measured recently suggests that closer scrutiny be given to the suggestion by Stockwell et al.[6] that acetylperoxy/peroxy chemistry as opposed to differential deposition velocities could explain the relative PAN versus O_3 removal rates.

References and Notes

(1) Stephens, E. R. *Adv. Environ. Sci. Technol.* **1969**, *1*, 119.

(2) Singh, H. B.; O'Hara, D.; Herlth, D.; Bradshaw, J. D.; Sandholm, S. T.; Gregory, G. L.; Sachse, G. W.; Blake, D. R.; Crutzen, P. J.; Kanakidou, M. A. *J. Geophys. Res.* **1992**, *97*, 16511.

(3) Roberts, J. M. *Atmos. Environ.* **1990**, *24A*, 243.

(4) Shepson, P. B.; Hastie, D. R.; So, K. W.; Schiff, H. I.; Wong, P. *Atmos. Environ.* **1992**, *26A*, 1259.

(5) Hartsell, B. E.; Aneja, V. P.; Lonneman, W. A. *J. Geophys. Res.* **1994**, *99*, 21033.

(6) Stockwell, W. R.; Milford, J. B.; Dongfen, G.; Yang, Y.-J. *Atmos. Environ.* **1995**, *29*, 1591.

(7) Gaffney, J. S.; Marley, N. A.; Drayton, P. Private communication.

(8) Niki, H.; Maker, P. D.; Savage, C. M.; Breitenbach, L. P. *J. Phys. Chem.* **1985**, *89*, 588.

(9) Moortgat, G. K.; Veyret, B.; Lesclaux, R. *Chem. Phys. Lett.* **1989**, *160*, 443.

(10) Horie, O.; Moortgat, G. K. *J. Chem. Soc., Faraday Trans.* **1992**, *88*, 3305.

(11) Maricq, M. M.; Wallington, T. J. *J. Phys. Chem.* **1992**, *96*, 986.

(12) Maricq, M. M.; Szente, J. J.; Kaiser, E. W. *J. Phys. Chem.* **1993**, *97*, 7970.

(13) Maricq, M. M.; Szente, J. J. *J. Phys. Chem.* **1996**, *100*, 12380.

(14) Lightfoot, P. D.; Cox, R. A.; Crowley, J. N.; Destriau, M.; Hayman, G. D.; Jenkin, M. E.; Moorgat, G. K.; Zabel, F. *Atmos. Environ.* **1992**, *26A*, 1805.

(15) DeMore, W. B.; Sander, S. P.; Golden, D. M.; Hampson, R. F.; Kurylo, M. J.; Howard, C. J.; Ravishankara, A. R.; Kolb, C. E.; Molina, M. J. *Chemical Kinetics and Photochemical Data for Use in Stratospheric Modeling*; JPL: Pasadena, CA, 1997; Publication 97-4.

(16) Maricq, M. M.; Szente, J. J. *J. Phys. Chem.* **1994**, *98*, 2078.

(17) Wallington, T. J.; Japar, S. M. *J. Atmos. Chem.* **1989**, *9*, 399.

(18) Tyndall, G. S.; Orlando, J. J.; Wallington, T. J.; Hurley, M. D. *Int. J. Chem. Kinet.* **1997**, *29*, 655.

(19) Chao, J.; Zwolinski, B. J. *J. Phys. Chem. Ref. Data* **1978**, *7*, 363.

(20) Unnumbered reactions in this table are of minor importance to the determination of k_1 . They are primarily included for completeness and for attempts to understand the anomalous nature of the "methylperoxy" concentrations determined from the UV absorbance measurements.

(21) Crawford, M. A.; Szente, J. J.; Maricq, M. M.; Francisco, J. S. *J. Phys. Chem.* **1997**, *101*, 5337.

(22) Delcroix et al. CMD meeting, Zurich, 1997.

(23) Maricq, M. M.; Szente, J. J. *J. Phys. Chem.* **1996**, *100*, 4507.

(24) Roehl, C. M.; Bauer, D.; Moortgat, G. K. *J. Phys. Chem.* **1996**, *100*, 4038.

(25) Moortgat, G. K.; Cox, R. A.; Schuster, G.; Burrows, J. P.; Tyndall, G. S. *J. Chem. Soc., Faraday Trans. 2* **1989**, *85*, 809.

(26) Veyret, B.; Lesclaux, R.; Rayez, M.-T.; Rayez, J.-C.; Cox, R. A.; Moortgat, G. K. *J. Phys. Chem.* **1989**, *93*, 2368.

(27) Andersson, B. Y.; Cox, R. A.; Jenkin, M. E. *Int. J. Chem. Kinet.* **1988**, *20*, 283.

(28) Atkinson, R.; Baulch, D. L.; Cox, R. A.; Hampson, R. F.; Kerr, J. A.; Troe, J. J. *J. Phys. Chem. Ref. Data.* **1997**, *26*, 521.

(29) Wallington, T. J.; Hurley, M. D.; Shi, J.; Maricq, M. M.; Sehested, J.; Nielsen, O. J.; Ellermann, T. *Int. J. Chem. Kinet.* **1993**, *25*, 651.

(30) Wallington, T. J.; Hurley, M. D. *Chem. Phys. Lett.* **1992**, *189*, 437.

(31) Koch, S.; Moortgat, G. K. *Chem. Phys. Lett.* **1990**, *173*, 151.

(32) Wallington, T. J.; Japar, S. M. *Chem. Phys. Lett.* **1990**, *166*, 495.

(33) Wayne, R. P. *Chemistry of Atmosphere*; Clarendon Press: Oxford, 1991.

(34) Stockwell, W. R.; Middleton, P.; Chang, J. S.; Tang, X. *J. Geophys. Res.* **1990**, *95*, 16343.

(35) Villalta, P. W.; Howard, C. J. *J. Phys. Chem.* **1996**, *100*, 13624.

(36) Sehested, J.; Christensen, L. K.; Møgelberg, T. E.; Nielsen, O. J.; Wallington, T. J.; Guschin, A.; Orlando, J. J.; Tyndall, G. S. *J. Phys. Chem.*, in press.